2018 IEEE/RSJ International Conference on Intelligent Robots and Systems (IROS)
Madrid, Spain, October 1-5, 2018

Sliding-layer laminates: a robotic material enabling robust and adaptable undulatory locomotion

Mingsong Jiang[1] and Nick Gravish[2]

Abstract— **Continuum robots that move through undulatory actuation must be composed of body materials that can enable flexible movement yet also provide resistive forces to the surrounding fluid, granular, or solid environments. This need for "flexible-yet-stiff" materials is notably important in robot designs that use passive propulsive elements such as tails and wings. Here we explore a laminate design paradigm for "flexible-yet-stiff" robotic materials through sliding layer laminates (SLLs). We present design principles motivated by theory and experiment and illustrate a taxonomy of SLL enabled morphable materials capable of up to 7 fold change in stiffness. Lastly, we demonstrate the applicability of SLLs to undulatory continuum robots: a swimming robot with a passive tail. We target two desired robot locomotor behaviors: fast open water swimming, and steady swimming through narrow channels emulating underwater caverns and pipes. We demonstrate how tuning the stiffness of the robot tail maximizes thrust generation in these two locomotion modes. Soft tails are optimal in confined swimming because they generate short amplitude high wavenumber oscillations, while stiff tails in confined environments either collide with the walls or do not generate sufficient thrust. However, stiff tails are far better in unconfined environments which enable large stroke amplitudes requiring high stiffness. Through this demonstration we show that stiff or soft tail designs alone are incapable of effective locomotion in complex underwater environments challenge.**

I. INTRODUCTION

Advances in robotics will be made through development of active, nonlinear, and unorthodox materials as building blocks [1], [2], [3]. Traditional robot materials have included rigid metals and plastics to compose the chassis, actuators, and manipulators [4], [5], [6]. Rigid systems thrive in industrial scenarios where precision is critical, however these robots present safety concerns in human-robot interactions and are limited in their adaptability and robustness in unstructured environments [7]. More recently soft-bodied robots have been developed with robot bodies and actuators composed of soft, flexible polymers [8], [9], [10]. Yet despite massive efforts in soft-robot design we still lack materials that are capable of rapid, repeatable, non-hysteretic, and low-energy variable compliance [11], [12], [13]. Tunable compliance materials may enable completely new functionalities to mobile robots and manipulation systems. For instance variable stiffness robot legs can enhance running robot performance [14].

Compliance modulation in robotics has been studied based on three main approaches, granular jamming effects, linear and non-linear spring designs, and through active material properties. The jamming phenomena can enable volumes or surfaces to increase in stiffness due to high internal friction forces generated by a controllable confining pressure. Two main approaches to jamming have been demonstrated. Granular jamming utilizes a membrane filled with frictional particles that when put under vacuum pressure generate internal friction and solidify [15]. Layer jamming uses layers of paper of other flat material which when put under pressure resist internal shear and thus resist bending [16]. Jamming systems have been used to develop variable stiffness medical devices [12], robotic grippers, and morphable structures [17]. While jamming is a versatile and impressive means of stiffness variation it is slow and requires cumbersome vacuum equipment. A more classic approach to stiffness variation is through machine design implementing linear and non-linear spring arrangements. Variable stiffness actuators, serial-elastic actuators, and other mechanisms that use kinematic linkages to make controllable stiffness systems [18], [19]. Lastly, there are many methods for compliance modulation that rely on active material properties such as dielectric-elastic polymers [20], [21].

A new and exciting direction for variable compliance in robot materials is through laminate and kirigami manufacturing methods [2], [22], [23], [24]. Recent work on the material properties of foldable and origami laminate systems has demonstrated a wide range of material behavior [25], [26]. In this paper we study a flat, variable compliance material fabricated through layer lamination with stiffness control enabled by layer sliding. These sliding layer laminates

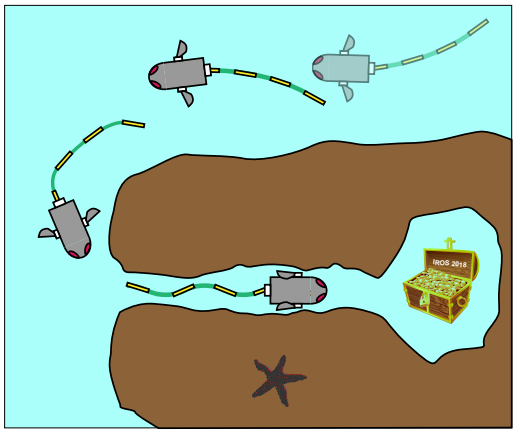

Fig. 1. Concept of a variable stiffness tail for an autonomous underwater vehicle capable of efficient propulsion in both open-water and confined environments.

These authors are with the [1]Department of Mechanical and Aerospace Engineering, University of California at San Diego. 9500 Gilman Dr, La Jolla, CA 92093 USA. Corresponding author ngravish@eng.ucsd.edu

Authorized licensed use limited to: Tsinghua University. Downloaded on August 25,2022 at 13:18:59 UTC from IEEE Xplore. Restrictions apply.

are inspired by a previous study of overlapping structured laminate layers which demonstrated the feasibility of the concept [27]. A goal of this is to implement the variable compliance into a bio-inspired swimming robot's tail which is then capable of safely and efficiently exploring through complex and changeable aquatic environments (Fig. 1).

II. CONCEPTUAL DESIGN & MODELING

The design of SLLs is motivated by a laminate layer that has periodic stiffness variation along their length. When multiple laminate layers with stiffness patterns are brought into or out of alignment, the whole beam bending stiffness can change dramatically (Fig. 2a). The stiffness variation phenomena can be understood through a simple cartoon model using parallel and series springs with different stiffness components (k_1 and k_2, with $k_1 >> k_2$). When the layers are aligned the composite stiffness of the system is dominated by the lower stiffness elements, and when the layers are anti-aligned the composite stiffness is higher due to the parallel configurations of the stiff and soft springs. However, unlike the spring analogy we can configure arrangements of layers over a continuum of overlapping states from 0% (anti-alignment) to 100% (perfect alignment) which potentially can lead to a continuum of stiffness variation in the composite beam (Fig. 2b). In this section we describe our modeling efforts to analytically design stiffness variation profiles in SLLs.

A. SLLs Multi-stiffness Modeling

Based on the dual-stiffness beam structure, we have developed a multi-stiffness model for SLLs. For simplicity we assume there is no relative sliding motion between layers under bending motions and the deflections are small compared to the length of the beam. We focus here on SLLs that contain only three layer-laminates, with the central laminate sliding between the top and bottom laminates for alignment re-configuration. However, this concept is extendable to an indefinite number of layers with periodic patterns along different longitudinal/horizontal directions.

Based on the periodic stiffness regions on each layered laminate, a sliding-layer mechanism can be achieved to create different alignment states between the soft and rigid regions, leading to different bending performances of the whole beam (Fig. 2b). To simplify the sliding-layer mechanism, we constrain the motion of both top and bottom laminates and change only the relative positions of the central laminate with regard to the outer laminates. Thus, the laminate alignment state is solely depended on the displacement of the central laminate. Due to the periodicity of the alignment states, the stiffness characterization of SLLs can be focused a single beam element with the alignment state varied from -100% (stiff) to 0% (soft) and back to 100% (stiff). We consider the $\pm 100\%$ range as opposed to the $0-100\%$ range because finite-size effects of the beams in experiment generate asymmetry between -100% to 100%. We use the alignment state as the input parameter to the modeling and assume that there is no layer sliding during beam bending,

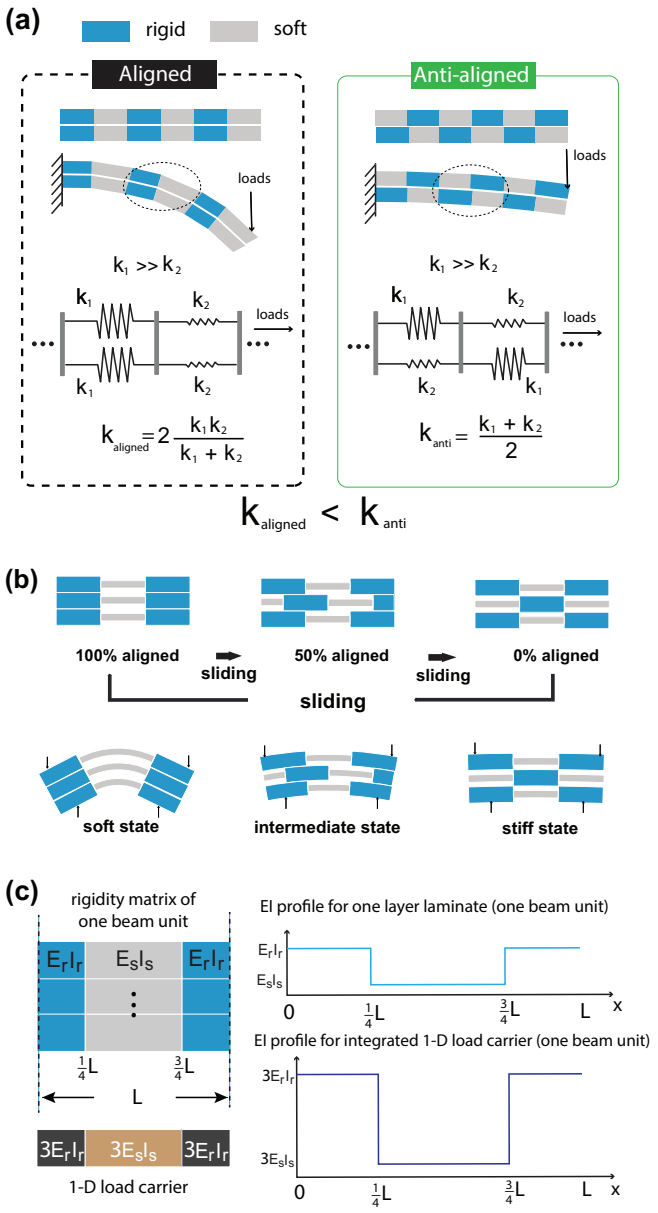

Fig. 2. Conceptual design of SLLs (a) A reconfigurable dual-stiffness structure analogized by a corresponding spring system. (b) Multi-stiffness enabled by a triple layered SLL with intermediate stiffness states. (c) Modelling of SLLs variable stiffness using integrated EI profiles (based on Euler-Bernoulli beam theory)

and thus the alignment state remains the same during the bending motion.

The modelling approach we have taken is based on Euler-Bernoulli beam theory and it provides a means of calculating the cantilever beam stiffness for beams with variable EI values. The Euler-Bernoulli equation describing the relationship between the beam's deflection and the applied loads is expressed as

$$\frac{d^2}{dx^2}(E(x)I(x)\frac{d^2\omega}{dx^2}) = q \tag{1}$$

where x is the horizontal position along the longitudinal direction, E is the Young's modulus (Pa), I is the second

Authorized licensed use limited to: Tsinghua University. Downloaded on August 25,2022 at 13:18:59 UTC from IEEE Xplore. Restrictions apply.

moment of area (m^4), ω is the transverse displacement of the beam at x and q is the distributed load (N/m). In this paper, we assume a clamped-free cantilever with a point load at the free end for stiffness characterization. We used $M(x)$, the bending moment, as the load source and rewrite (1) as

$$M(x) = E(x)I(x)\frac{d^2\omega(x)}{dx^2} \tag{2}$$

Additionally, the deflection at each point along x can be integrated for a total displacement at the beam's free end, which can be expressed as

$$y = \int\int_L \frac{M(x)}{E(x)I(x)} dxdx \tag{3}$$

where y is the total tip displacement at the free end and L is the total length of the beam. The effective spring stiffness of an elastic beam can be expressed as

$$K = \frac{P}{y} \tag{4}$$

Based on the cantilever beam bending test, we have

$$M(x) = P(L-x) \tag{5}$$

By inserting (3) and (5) into (4) we have,

$$K = \frac{P}{\int\int_L \frac{P(L-x)}{E(x)I(x)dxdx}} = \frac{1}{\int\int_L \frac{(L-x)}{E(x)I(x)dxdx}} \tag{6}$$

Thus, the bending stiffness of beam with variable flexural rigidity can be expressed as (6). For SLLs with different longitudinal alignment states across multiple layered laminates in the transverse direction, the flexural rigidity can be simplified as the addition of multiple EIs at each longitudinal position x [28]. This is expressed as

$$E(x)I(x)_{int} = \sum_{i=1}^{n} E(x)_i I(x)_i \tag{7}$$

where $E(x)I(x)_{int}$ is the total flexural rigidity for all the composite beam elements at the same longitudinal position x and i stands for each composite layer. We then replace each soft and rigid region with EI values and combine them as a 1-D load carrier (Fig. 2c).

Based on (7), we integrate the flexural rigidity in the column-wise direction to generate an effective 1D-load carrier with EIs along the longitudinal direction x. By changing α, the alignment percentage, we can achieve different rigidity matrices within the same SLL beam unit, which forms different EI profiles of the 1D-load carrier (Fig. 2c left). Finally, we extract the varying EI values from each individual laminate and integrate them as EI profiles (EI changing as a function of x) for the 1-D load carrier (Fig. 2c right). Finally, the $E(x)I(x)$ from (6) can be determined by the integrated EI profiles for calculating the effective spring stiffness at the tip end for any alignment state of the SLLs.

B. Design Principles in Possible Stiffness Variations

The effective bending stiffness at the SLL tip is closely related with the EI profiles under different alignment states. In this part, we introduce two design principles to discuss possible EI profiles and investigate different paths for stiffness-alignment curvatures. The design principles we focus on are: 1) material choices of SLLs, defined as changing the flexural rigidities of the soft and rigid regions. 2) The aspect ratio of rigid and soft regions, defined as changing the length of the rigid region in proportion to the whole length of one beam unit. In our computational analysis the SLLs contain 100 beam units (EI periods) with each unit the length of a non-dimensional unit length 1.

We first characterize the influence of changing the material composition on either rigid or soft stiffness regions separately shown in Fig. 3a and b. By increasing the young's modulus of the stiff regions (E_rI_r) while keeping constant the soft region material properties (E_sI_s), we observe that the 0% alignment state stiffness increases linearly while the $\pm$100% state stiffness marginally changes (Fig. 3a). The inset shows the stiffness gain of the stiff and soft alignment states with changing E_rI_r. On the other hand, increasing E_sI_s while keeping E_rI_r results in a linear increase in the $\pm$100% stiffness with the stiffest state stiffness remaining relatively unchanged (Fig. 3b). These calculations reveal that material selection for SLLs governs the stiffness variation range of the SLL structure. Note that a symmetric stiffness variation is guaranteed for SLLs with many (>10) beam units but when we compare to experiment we will see this symmetry disappears.

Next, based on different aspect ratios (ARs), we changed the overlapping areas between the inner and outer rigid regions from all layers. Through control of aspect ratio we control the sensitivity of the stiffness variation with alignment state (Fig. 3c). With AR = 50% the stiffness gradually changed while at higher aspect ratio a high stiffness is maintained over a long range of inner layer displacement. The elongated rigid regions (shortened soft regions) increased the SLL stiffness on both ends (stiffest and softest states). Such a result reveals the fundamental role of aspect ratio in changing the sensitivity of the SLL stiffness-alignment curvatures, where beam stiffness could be modulated either in a graded (continuum) fashion or as a binary material property (stiff or soft).

III. FABRICATION

The fabrication process of the SLLs was based on conventional laser cutting [2], as illustrated in Fig. 4. Structural layers (FR-4 glass fiber, thickness: 0.12-0.50mm), compliant films (Kapton, thickness: 12-50μm), adhesive layers (double-sided pressure-sensitive-adhesive films, thickness: 3μm) and boundary layers (adhesive thin or thick tapes) are necessary for the fabrication of multi-stiffness SLL structures. Each layer is designed with its own beam profile to achieve periodic stiffness patterning in one layered laminate (Fig. 4a).

Authorized licensed use limited to: Tsinghua University. Downloaded on August 25,2022 at 13:18:59 UTC from IEEE Xplore. Restrictions apply.

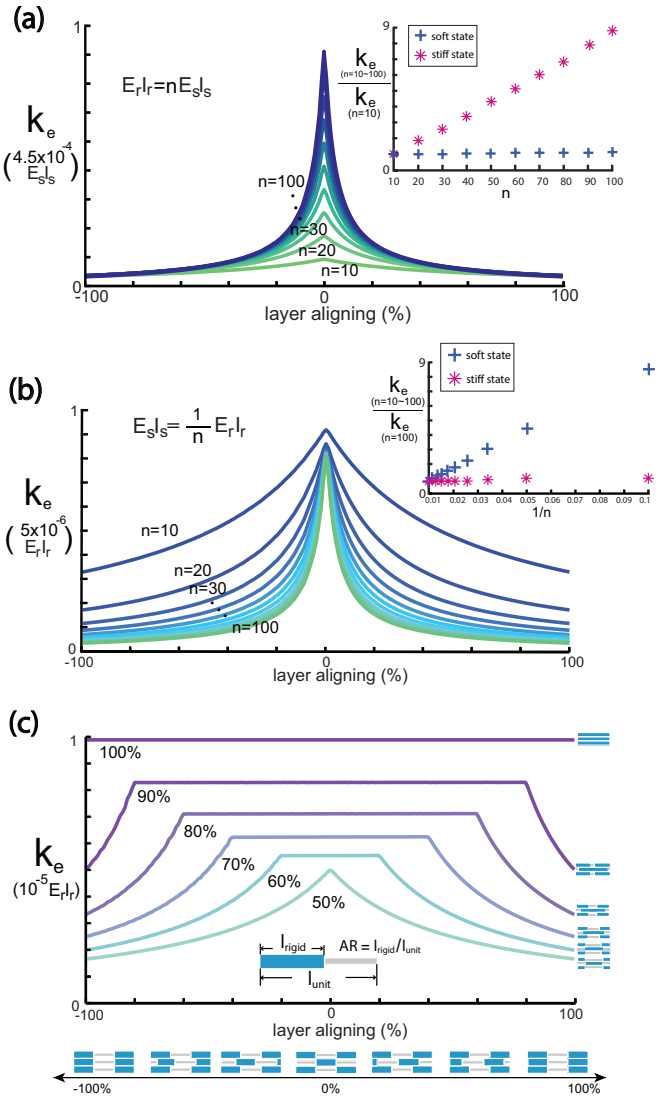

Fig. 3. Effective bending stiffness modeling from SLLs containing 100 beam units using cantilever beam test based on Euler-Bernoulli beam theory (a) Varying $E_rI_r = nE_sI_s$ (n= 10,20,...,100) (b) Varying $E_sI_s = \frac{1}{n}E_rI_r$ (n=10,20,...,100) (c) Changing beam aspect ratio from 50% to 90%.

Individual lamination for one layered laminate combines laser cutting, precision alignment with dowel pins, and adhesive bonding using a hydraulic press. This process is divided into 4 consecutive steps, individual material cuts, layer alignment, final cuts, and final release (Fig. 4b). We first cut all composite layers (the structural/adhesive/compliant) with stiffness patterning and alignment holes. To form a central layer that will slide without binding we laminate this layer with compliant films on the top and bottom of the laminate. We then align all the individual layers using dowel pins and adhere the pressure sensitive adhesive in a hydraulic press. We then place the SLL back in the laser and perform the final cut of the laminated layer. This is done by alignment of the laser head with each corner of the SLL piece and we cut with a higher power density. Note that double sided compliant films might cause buckling effects and thus we used very thin Kapton (25.5μm) films where buckling does not affect the bending performance of the SLLs.

Following the same steps as the central layer, we prepared the outer laminates with the same stiffness patterning. To fix the motion of the outer laminates, two layer-boundaries have to be positioned on the sides to generate a continuous bending motion. Once the outer layers are bonded we insert the central layer into the SLL with (Fig. 4c). A prototype using FR-4 and Kapton flexures is shown with different alignment state and bending performance in Fig. 4d.

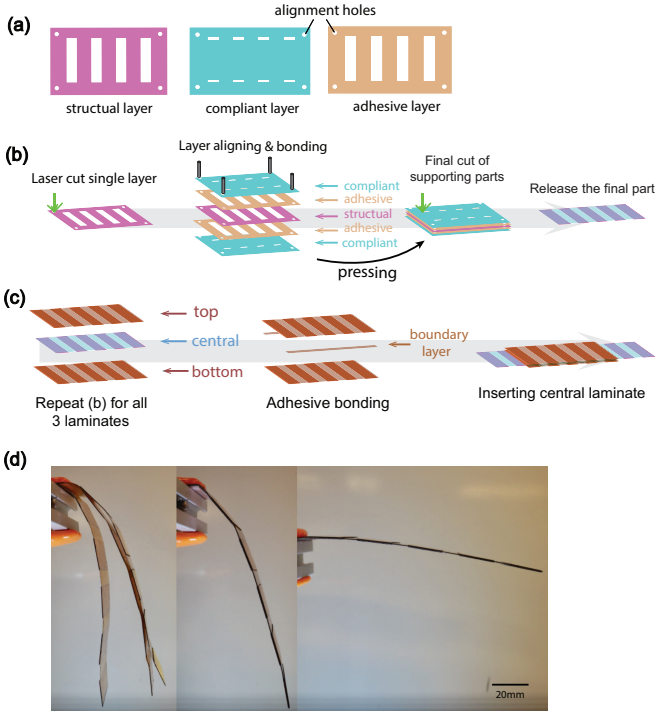

Fig. 4. The lamination process in SLLs fabrication (a) Beam profiles for each composite layer within one laminate (b) Steps for making one layered laminate (c) Steps for integrating a SLLs' beam structure (d) bending stiffness comparison of a SLLs' prototype including no boundary layers (left), with boundary layes in soft state (middle) and with boundary layers in stiff state (right).

IV. RESULTS & DISCUSSIONS

A. Experimental Setup

The bending stiffness of SLLs is characterized using the fixed end cantilever beam tests, shown in Fig. 5a. Instead of having a long SLL as a test specimen, here we focused on measuring the stiffness variation from a single beam unit of an SLL to have observable force readings under a small tip deflection range (Euler-Bernoulli beam theory). The effective bending stiffness of the specimen is then defined as the deflection force from a load cell (100g micro load cell, Phidgets) divided by the deflection distance controlled by a linear stage (Thorlabs). Specifically, we fix the SLL onto a stationary stage while driving the load cell against the SLL using a motorized linear stage. The linear translation is controlled by a stepper motor (Oriental Motor, PK546PMB) connected to the stage using a flexible coupling (SDP/SI) connected with a machined coupler. We measured

Authorized licensed use limited to: Tsinghua University. Downloaded on August 25,2022 at 13:18:59 UTC from IEEE Xplore. Restrictions apply.

the effective bending stiffness based on a series of laminate alignments and compared with the modelling stiffness based on two design principles.

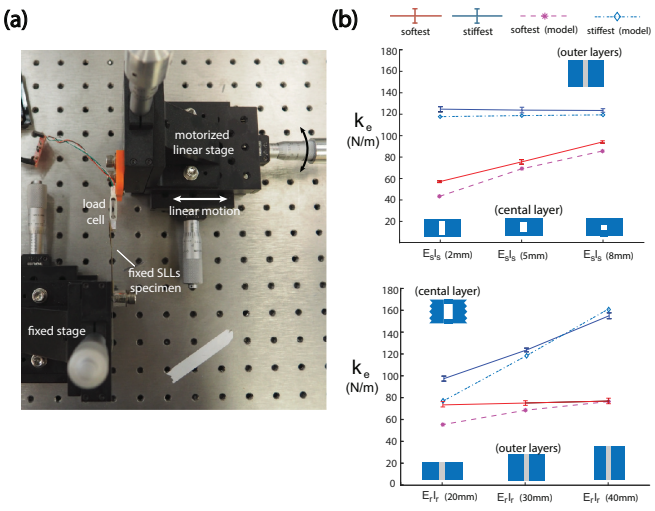

Fig. 5. Experimental testing of SLLs effective bending stiffness (a) Cantilever beam bending stiffness measured using SLLs specimen (one beam unit) fixed on a stationary stage with one load cell driven by a motorized linear stage. (b) results from changing flexural rigidities of soft and rigid regions compared with the modelling. The data summarize the results of stiffness tests over five individual experiments.

B. Results from Changing the E_rI_r and E_sI_s

As predicted by the modelling, changing E_rI_r significantly affected the stiffness of the SLL in the stiff states with little influence on the soft states' stiffness; while changing E_sI_s changed the stiffness in the soft state with little effect on the stiff state stiffness. This test experimentally demonstrates that to separately control the stiff and soft states one can do so by selectively changing the flexural rigidities from the stiff and soft beam regions. Furthermore, these results show excellent agreement with the predictions from our theory developed in previous sections. The theoretical predictions have no fitting parameters with equation constants solely based on material properties, thus showing excellent agreement between experiment and theory.

Changes to the SLLs beam width of the rigid and soft regions will also change the effective cross-sectional moment of area, I, and thus will manipulate the flexural rigidity of the two stiffness regions. The designs we used are all 40 mm in length, with 2mm, 5mm and 8mm the beam width of the soft regions and 20mm, 30mm, 40mm the beam width of the rigid regions. In Fig. 5b, we observe a linearly increased bending stiffness in the soft state by keeping the E_rI_r (30mm) while changing the E_sI_s (2/5/8mm). On the other hand, by keeping E_sI_s and changing E_rI_r, we observed a linear stiffness increase in the stiff state but little variation of the soft state. The experiment results are an average over 5 independent stiffness tests and the predicted stiffness is based on the EI profile modelling, which strongly agrees with the testing results without any fitting factors.

C. Results from Changing the Aspect Ratio

The change of aspect ratios is an important design principle for changing the sensitivity of the stiffness variation. To validate this design principle, we fabricated one beam unit SLL specimens with the same material choices (FR-4 0.25mm, Kapton 25.5 μm). Each beam unit of the outer layers is 40mmx40mm whereas each one of the central layer is 36mmx40mm (2mm width of boundary layers on each side). From aspect ratio 50% to 90%, we changed the length of the rigid regions in portion of the length of one beam unit while keeping the same values of E_rI_r and E_sI_s (Fig. 6 upper left).

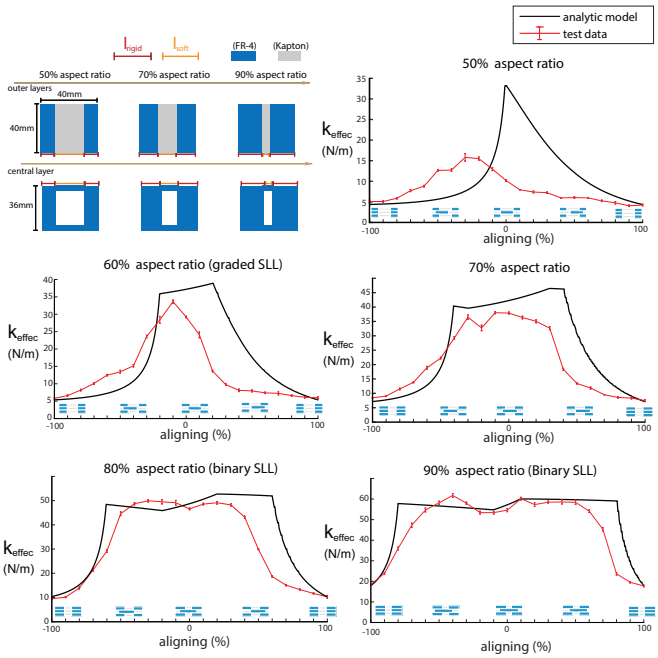

Fig. 6. Effective bending stiffness of SLLs based on different aspect ratios. The experimental data summarize the results of stiffness tests over five individual experiments.

In Fig. 6, each figure exhibits the stiffness-alignment curvature of SLLs with different aspect ratios. With the increasing aspect ratio, the stiffness of both the stiffest and softest states rose approximately 3 times (from 50% to 90%); however, as we increase the aspect ratio the stiffness stays in the stiff for larger alignment displacements. This affects the sensitivity of the stiffness variation against the sliding motion. Such a feature can be used for designing either graded (60%) or binary SLLs ($80-90\%$) where stiffness variation and sensitivity can be tailored for different applications. For instance, the binary SLL can be used in areas where the variable stiffness is desired for an on-off pattern with the on-state stiffness as high as possible. Since the transition between the on to off state is shorter, the actuation requirements would require less displacement and thus less energy consumption; while the graded SLL can be used for cases where stiffness has to be gradually changed using continuous actuation methods. Consequently, the difficulty of the linear sliding motion will increase with the decreasing

Authorized licensed use limited to: Tsinghua University. Downloaded on August 25,2022 at 13:18:59 UTC from IEEE Xplore. Restrictions apply.

size of the SLLs' design. As a comparison, the predicted stiffness with only one SLLs' beam unit strongly agrees with the experimental results in high aspect ratios. For low aspect ratio (50%), the model overestimates the data due to the 3D design imperfections leading to a discontinuous bending curvature of the stiffest state.

V. DEMONSTRATION

A. SLLs enable optimal swimming propulsion in both open and confined underwater environments

We have so far considered SLLs as an abstract material capable of stiffness variation. We now seek to use this stiffness control for a flapping tail of a autonomous underwater vehicle (AUV) concept (Fig. 1). We hypothesize that variable mechanical stiffness of a fish-inspired AUV tail will enable high functionality for exploring complex and confined underwater environments. Our bio-inspired approach is motivated by biological observations in which fish swimming performance under different driving conditions is optimized for different tail stiffness [29], [30]. In this paper, we considered SLLs as a passive tail and we target two desired robot locomotion patterns: high-frequency and amplitude open water swimming, and low-frequency, low amplitude swimming through a confined tunnel (or pipe).

We first consider SLLs with dual-compliance states flapping under two driving amplitudes (high and low) and measured the thrusts using a load cell. The thrust is measured over a range of frequency from 2-5 hz. We measured thrusts using a robotic swimmer confined to move along a linear trackway. Driven by a stepper motor (Oriental Motor, PK546PMB), the SLLs oscillation creates thrusts and drives the robot forward on the trackway eventually reaching a load cell (Fig. 7a). We used a solenoid to actuate the central layer of the SLL to dynamically control the alignment state. We performed thrust measurements over a range of frequencies and amplitudes and recorded the averaged forces from the load cell. The SLLs tails are fabricated using FR-4 (0.685mm ,0.787mm), Kapton (0.05mm) and Mylar (0.178mm) (Fig. 7b). For the outer case (104mm x 40mm), we chose a half laminated design where only one layer of Kapton (0.05mm) and FR-4 (0.685mm) are laminated together with the Kapton facing inward for a smooth sliding interface. The central laminate (137mm x 32mm) is a full laminated design with two layers of Mylar (0.178mm, $E-0.199Gpa$) covering the FR-4 (0.787mm). Here the soft regions are cut into one strip of Mylar (beam width 3mm), such as to have both an observable stiffness change and easy pull and push sliding motion. Here we demonstrate that by undergoing pure self-weight, the tip displacement difference of two stiffness states are about 4 folds, meaning that the effective bending stiffness from the stiff state is around 5 times the one in the soft state (Fig. 7c,d). A picture of the experimental designs is shown in Fig. 7e.

Based on all the parameter settings, we drove the SLLs under the two extreme stiffness states and measured the thrusts using a load cell over a range of driving conditions, where the raw data displays the change in thrust generations shown in Fig. 8a. Fig. 8b shows two sets of comparisons of thrust generation between the stiff and soft state SLLs in both a low ($\pm 7.2^\circ$) and a high driving amplitude ($\pm 14.4^\circ$) over a range of driving frequencies (from 2 hz to 5 hz). As we measured thrusts under a low amplitude ($\pm 7.2^\circ$), the stiffest state SLLs is better than the softest state SLLs in thrust generation in low frequency regimes; however, by increasing the driving frequency, the thrusts generated by the softest state SLLs are increased and comparable with the thrusts by the stiffest state SLLs (Fig. 8b top). The data is based on 5 independent tests with averaged value and standard deviations. On the other hand, as we repeated the same experiments under a higher driving amplitude ($\pm 14.4^\circ$), two different thrust peaks are exhibited for both the stiff and soft state SLLs, where the stiff state SLLs can be effective in thrust generation around 4hz and 3hz for the soft state SLLs (Fig. 8b bottom). This indicates that an optimized swimming speed or force is related with the combination of driving conditions and the tail stiffness, and thus the variable stiffness SLL can be exploited for improved swimming performance as a response to each variable working and driving condition.

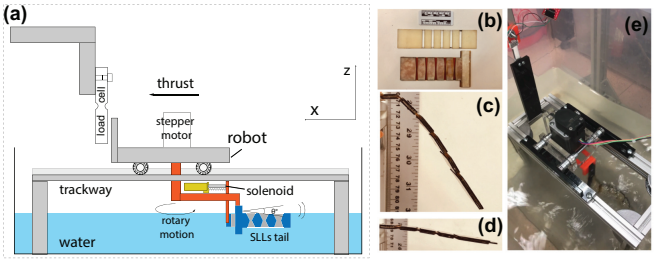

Fig. 7. Measuring thrusts from a wheeled and tailed robot driven by SLLs flapping motions (using a stepper motor). (a) Experimental setups for thrusts measurement. (b) SLLs tail prototype (c)(d) are bending performances between stiff and soft states. (e) Isometric view of the water-track experimental platform.

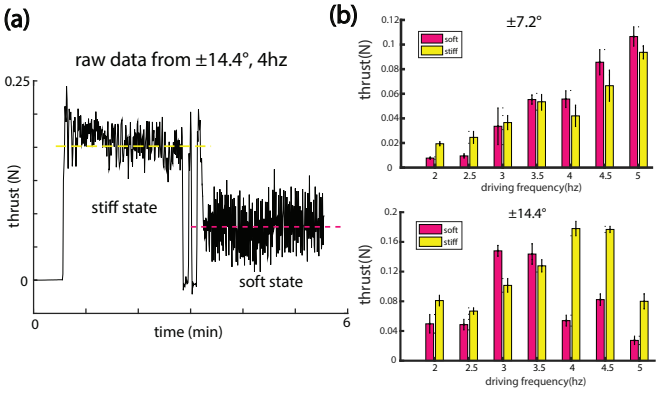

Fig. 8. Thrusts measured from SLLs flapper under two sets of driving conditions. (a) Raw data from one driving condition of one test. Here we used solenoid for changing beam stiffness and thrust generations. (b) Results from sweeping amplitudes $\pm 7.2^\circ$ over 2-5Hz. (c) Results from sweeping amplitudes $\pm 14.4^\circ$ 2-5Hz. The data summarize the results of thrusts (N) over five individual experiments.

Authorized licensed use limited to: Tsinghua University. Downloaded on August 25,2022 at 13:18:59 UTC from IEEE Xplore. Restrictions apply.

B. Open-water vs. Confined space undulatory swimming performances

Based on the previous measurement of the thrust generations from SLLs' passive propulsor under 2 different states, we proposed another use of variable compliance SLLs navigating through structured aquatic environments. Specifically, we hypothesize that a high-frequency swimming pattern in open water would be optimized by the high-stiffness SLL state, and a slow but steady swimming pattern through a narrowed confined space would be optimized by the soft stiffness SLLs state. To demonstrate this, we exploited the same design concept by using a double-rail system with a longer SLLs as a passive propulsor (Fig. 9a). In the system, 2 sliders combined with a acrylic plate consists of the base of the swimmer, where the SLLs are connected with the stepper motor using a coupler to generate thrusts in the water. As a demonstration, we drove the swimming robot in both a open water scenario (in a water tank) and a narrowed channel space (45 x 392mm, with 2 acrylic plates sitting on the bottom of the tank as the walls) (Fig. 9b). We then tracked positions of the tails and sliders along the rail system and observed the swimming performance. Figure 10 illustrates the performances of the robotic swimmer navigating through these environments. Note that a high sweeping amplitude will increase the thrust generation[29], we choose a high sweeping amplitude to maximize the thrust. In the open water, stiff state SLLs can generate powerful strokes with a high sweeping amplitude ($\pm 72^{\circ}$)), which can easily navigate along the rail system (Fig. 10a); however, a soft state SLLs driven with the same condition will not be efficient enough to glide through the rail system. On the other hand, as we built the walls and restricted the flapping motion of the SLLs tail, the soft state SLLs is found useful in generating low amplitude ($\pm 21.6^{\circ}$) steady motion through the channel whereas the stiff state can only pass through the first half of the channel as the tail's end is hitting onto the acrylic walls (Fig. 10b). This can be explained by the physical interference between the tail and walls combined with suction effects caused by the stiff SLL tails pushing water to the sides which bounces back to the stiff state SLLs. Since more water is pushed to the sides instead of backwards, the total thrust generated is less. The results from the robotic swimmer indicate a potential application for variable stiffness passive propulsors and robots to operate inside complex aquatic environments.

VI. CONCLUSION

In summary, we have demonstrated that the sliding-layer mechanism of laminates can be exploited to create flexible and morphable materials with variable beam compliance that can be integrated into mobile robots as passive appendages achieving undulatory locomotion through multi-modal environments. Although many have proposed variable stiffness structures using spring systems (virtual spring), jamming effects, and electroactive materials in recent years, we believe that the SLL approach proposed and studied here opens avenues for the design of new class of multi-functional

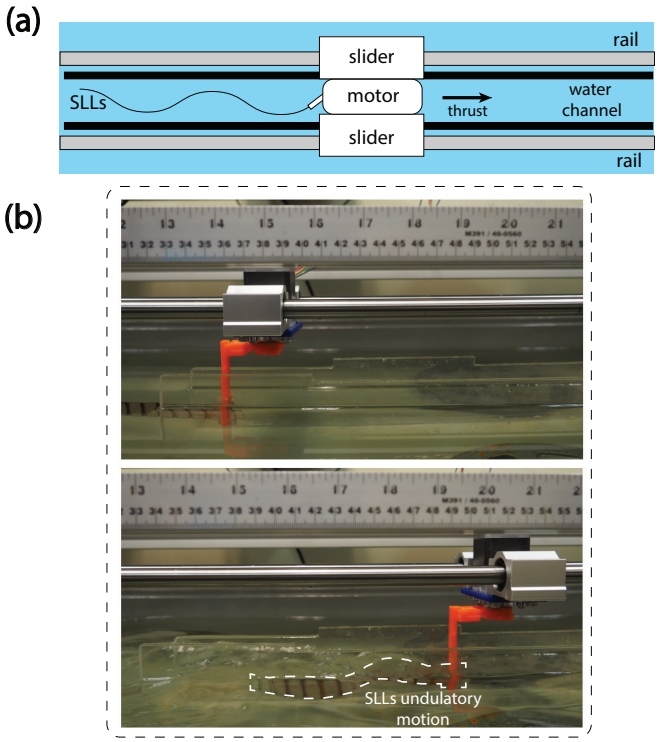

Fig. 9. Setups for rail-based SLLs robotic swimmer (a) Diagrams of robotic swimmer swimming through a confined channel using SLLs tail from top view (b) Robotic swimmer passing through a confined channel based on undulatory motion of the SLLs propulsor (driven by a stepper motor).

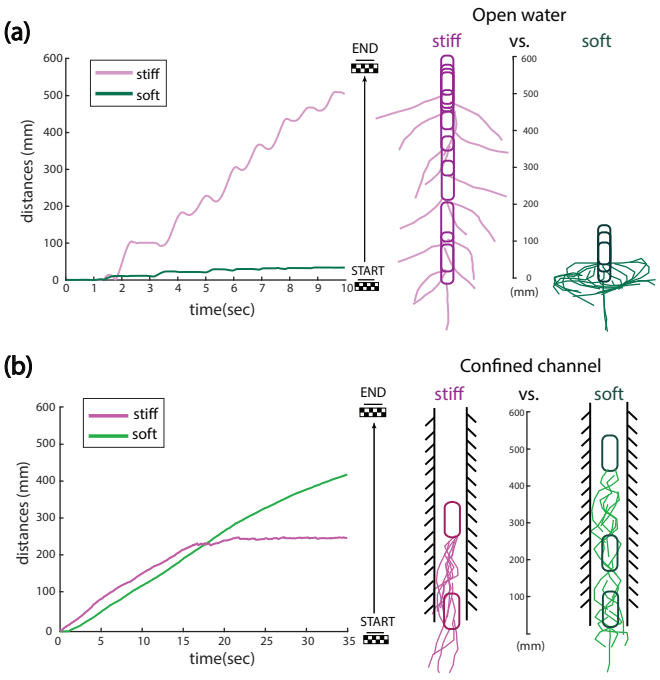

Fig. 10. Tracking of robotic swimmer under a dual aquatic environments (a) Open-water high amplitude swimming pattern (tracking every 0.67 seconds). (b) Confined space steady speed swimming pattern (tracking every 3 seconds).

Authorized licensed use limited to: Tsinghua University. Downloaded on August 25,2022 at 13:18:59 UTC from IEEE Xplore. Restrictions apply.

materials enabling robust and adapatble undulatory locomotors that can travel through complex environments for search and rescue, exploration and inspection, environmental monitoring, and medical procedures.

ACKNOWLEDGMENT

We thank Mike Tolley and Mike Yip for comments and discussion.

REFERENCES

[1] Yiğit Mengüç, Nikolaus Correll, Rebecca Kramer, and Jamie Paik. Will robots be bodies with brains or brains with bodies? *Science Robotics*, 2(12):eaar4527, 2017.

[2] Samuel Felton, Michael Tolley, Erik Demaine, Daniela Rus, and Robert Wood. A method for building self-folding machines. *Science*, 345(6197):644–646, 2014.

[3] Filip Ilievski, Aaron D Mazzeo, Robert F Shepherd, Xin Chen, and George M Whitesides. Soft robotics for chemists. *Angewandte Chemie*, 123(8):1930–1935, 2011.

[4] Kevin C Galloway, Galen Clark Haynes, B Deniz Ilhan, Aaron M Johnson, Ryan Knopf, Goran A Lynch, Benjamin N Plotnick, Mackenzie White, and Daniel E Koditschek. X-rhex: A highly mobile hexapedal robot for sensorimotor tasks. 2010.

[5] Mourad Bouzit, Grigore Burdea, George Popescu, and Rares Boian. The rutgers master ii-new design force-feedback glove. *IEEE/ASME Transactions on mechatronics*, 7(2):256–263, 2002.

[6] Andrea Caffaz and Giorgio Cannata. The design and development of the dist-hand dextrous gripper. In *Robotics and Automation, 1998. Proceedings. 1998 IEEE International Conference on*, volume 3, pages 2075–2080. IEEE, 1998.

[7] Sebastian Wolf and Gerd Hirzinger. A new variable stiffness design: Matching requirements of the next robot generation. In *Robotics and Automation, 2008. ICRA 2008. IEEE International Conference on*, pages 1741–1746. IEEE, 2008.

[8] Daniela Rus and Michael T Tolley. Design, fabrication and control of soft robots. *Nature*, 521(7553):467, 2015.

[9] Deepak Trivedi, Christopher D Rahn, William M Kier, and Ian D Walker. Soft robotics: Biological inspiration, state of the art, and future research. *Applied bionics and biomechanics*, 5(3):99–117, 2008.

[10] Carmel Majidi. Soft robotic: a perspective-current trends and prospects for the future. *Soft Robotics*, 1(1):5–11, 2014.

[11] M Manti, V Cacucciolo, and M Cianchetti. Stiffening in soft robotics: A review of the state of the art. *IEEE Robot. Autom. Mag.*, 23(3):93–106, 2016.

[12] Sangbae Kim, Cecilia Laschi, and Barry Trimmer. Soft robotics: a bioinspired evolution in robotics. *Trends in biotechnology*, 31(5):287–294, 2013.

[13] Carmel Majidi and Robert J Wood. Tunable elastic stiffness with microconfined magnetorheological domains at low magnetic field. *Applied Physics Letters*, 97(16):164104, 2010.

[14] Kevin C Galloway, Jonathan E Clark, Mark Yim, and Daniel E Koditschek. Experimental investigations into the role of passive variable compliant legs for dynamic robotic locomotion. In *Robotics and Automation (ICRA), 2011 IEEE International Conference on*, pages 1243–1249. IEEE, 2011.

[15] Eric Brown, Nicholas Rodenberg, John Amend, Annan Mozeika, Erik Steltz, Mitchell R Zakin, Hod Lipson, and Heinrich M Jaeger. Universal robotic gripper based on the jamming of granular material. *Proceedings of the National Academy of Sciences*, 107(44):18809–18814, 2010.

[16] Jifei Ou, Lining Yao, Daniel Tauber, Jürgen Steimle, Ryuma Niiyama, and Hiroshi Ishii. jamsheets: thin interfaces with tunable stiffness enabled by layer jamming. In *Proceedings of the 8th International Conference on Tangible, Embedded and Embodied Interaction*, pages 65–72. ACM, 2014.

[17] Elliot Hawkes, B An, Nadia M Benbernou, H Tanaka, S Kim, ED Demaine, D Rus, and Robert J Wood. Programmable matter by folding. *Proceedings of the National Academy of Sciences*, 107(28):12441–12445, 2010.

[18] Riccardo Schiavi, Giorgio Grioli, Soumen Sen, and Antonio Bicchi. Vsa-ii: A novel prototype of variable stiffness actuator for safe and performing robots interacting with humans. In *Robotics and Automation, 2008. ICRA 2008. IEEE International Conference on*, pages 2171–2176. IEEE, 2008.

[19] Giovanni Tonietti, Riccardo Schiavi, and Antonio Bicchi. Design and control of a variable stiffness actuator for safe and fast physical human/robot interaction. In *Robotics and Automation, 2005. ICRA 2005. Proceedings of the 2005 IEEE International Conference on*, pages 526–531. IEEE, 2005.

[20] Hiroya Imamura, Kevin Kadooka, and Minoru Taya. A variable stiffness dielectric elastomer actuator based on electrostatic chucking. *Soft matter*, 13(18):3440–3448, 2017.

[21] Atsuo Orita and Mark R Cutkosky. Scalable electroactive polymer for variable stiffness suspensions. *IEEE/ASME Transactions on Mechatronics*, 21(6):2836–2846, 2016.

[22] J P Whitney, P S Sreetharan, K Y Ma, and R J Wood. Pop-up book MEMS. *J. Micromech. Microeng.*, 21(11):115021, 2011.

[23] Cagdas D Onal, Robert J Wood, and Daniela Rus. Towards printable robotics: Origami-inspired planar fabrication of three-dimensional mechanisms. In *Robotics and Automation (ICRA), 2011 IEEE International Conference on*, pages 4608–4613. IEEE, 2011.

[24] Sina Sareh and Jonathan Rossiter. Kirigami artificial muscles with complex biologically inspired morphologies. *Smart Materials and Structures*, 22(1):014004, 2012.

[25] Kazuko Fuchi, Alejandro R Diaz, Edward J Rothwell, Raoul O Ouedraogo, and Junyan Tang. An origami tunable metamaterial. *Journal of Applied Physics*, 111(8):084905, 2012.

[26] Jesse L Silverberg, Arthur A Evans, Lauren McLeod, Ryan C Hayward, Thomas Hull, Christian D Santangelo, and Itai Cohen. Using origami design principles to fold reprogrammable mechanical metamaterials. *science*, 345(6197):647–650, 2014.

[27] Yong-Jai Park, Jong-Gu Lee, Sangwon Jeon, Heejin Ahn, Jesung Koh, Junghyun Ryu, Maenghyo Cho, and Kyu-Jin Cho. Dual-stiffness structures with reconfiguring mechanism: Design and investigation. *Journal of Intelligent Material Systems and Structures*, 27(8):995–1010, 2016.

[28] Jonas Bareisis. Stiffness and strength of multilayer beams. *Journal of composite materials*, 40(6):515–531, 2006.

[29] Matthew J McHenry, Charles A Pell, and JH Long. Mechanical control of swimming speed: stiffness and axial wave form in undulating fish models. *Journal of Experimental Biology*, 198(11):2293–2305, 1995.

[30] Eric D Tytell, Megan C Leftwich, Chia-Yu Hsu, Boyce E Griffith, Avis H Cohen, Alexander J Smits, Christina Hamlet, and Lisa J Fauci. Role of body stiffness in undulatory swimming: insights from robotic and computational models. *Physical Review Fluids*, 1(7):073202, 2016.

Authorized licensed use limited to: Tsinghua University. Downloaded on August 25,2022 at 13:18:59 UTC from IEEE Xplore. Restrictions apply.